



Effects of electrodes and imposed flow on forced ignition in laminar premixed hydrogen/air mixtures with large Lewis number

Xinyi Chen^a, Shumeng Xie^a, Hannes Böttler^b, Arne Scholtissek^b,
Wang Han^c, Dehai Yu^a, Christian Hasse^b, Zheng Chen^{a,*}

^a SKLTCS, CAPT, BIC-ESAT, College of Engineering, Peking University, Beijing 100871, China

^b Institute for Simulation of reactive Thermo-Fluid Systems, TU Darmstadt, Otto-Berndt-Straße 2, 64287 Darmstadt, Germany

^c School of Engineering, The University of Edinburgh, Edinburgh, Scotland EH8 3JL, UK

Received 3 January 2022; accepted 22 July 2022

Available online xxx

Abstract

Compared to quiescent premixed reactants, forced ignition of flowing/turbulent premixed reactants is expected to be more difficult because of increased dissipation of the deposited energy. However, the counterintuitive turbulence-facilitated ignition (TFI) has been observed in recent experiments for mixtures with large Lewis number, Le . The mechanisms behind TFI are still not well understood and this study aims to interpret a part of the TFI mechanisms through considering electrodes and imposed flow in the simulations of forced ignition in hydrogen/air mixtures. The imposed flow emulates the local turbulent effects around the electrodes which might blow the ignition kernel away from the electrodes. Since TFI occurs only for mixtures with large Le (e.g., lean hydrocarbon/air or rich H_2 /air mixture), a fuel-rich ($\phi=5.1$) H_2 /air mixture with $Le\approx 2.3$ is investigated to reduce computational cost and consider more factors that may lead to TFI. Similar to TFI observed in experiments, the flow-facilitated ignition is observed for H_2 /air with $\phi=5.1$ and $Le\approx 2.3$ when the electrodes have a small gap distance. The detailed effects of including electrodes on forced ignition of quiescent and flowing mixtures are explored. It is found that the existence of electrodes not only induces heat loss but also affects the shape and global curvature/stretch of the ignition kernel. The heat loss to the electrodes is demonstrated to play an important role for the ignition of mixtures with large Le . Compared to quiescent mixtures, considering an imposed flow normal to the electrodes can blow the flame kernel away from the cold electrodes. Such movement of the ignition kernel can greatly reduce both the heat loss to the electrodes and flame curvature/stretch, and thereby promote the ignition in mixtures with large Le . These results help to understand the underlying mechanisms for the TFI observed in experiments.

© 2022 The Combustion Institute. Published by Elsevier Inc. All rights reserved.

Keywords: Ignition; Lewis number; Heat loss; Flame curvature; Hydrogen

* Corresponding author.

E-mail address: cz@pku.edu.cn (Z. Chen).

<https://doi.org/10.1016/j.proci.2022.07.217>

1540-7489 © 2022 The Combustion Institute. Published by Elsevier Inc. All rights reserved.

1. Introduction

Spark ignition is the most common approach to initiate the combustion process in many practical combustion devices, such as gasoline engines and gas turbine engines. In these engines, ignition must occur in turbulent flows [1]. Moreover, increasingly stringent regulations on engine emission and fuel economy have driven a trend towards combustion under extreme conditions (e.g., ultra-lean combustion [2,3]). Under such conditions, the mixtures are less reactive and more difficult to be ignited. To address these challenges, it is crucial to understand the fundamental mechanisms controlling ignition processes in turbulent flows [1].

In the literature, there are many fundamental studies on premixed flame ignition in turbulent flows. Usually turbulence inhibits ignition since it increases the dissipation rate of the deposited energy for ignition kernel development [4]. Such inhibiting effects were demonstrated by many experiments [5–10] and simulations [11–13]. For example, Shy and co-workers [5–9] and Cardin et al. [10] reported the minimum ignition energy (MIE) transition with the increase of turbulent intensity based on ignition measurements in two types of turbulent flows. They found that the MIE increases slightly (abruptly) with turbulence intensity before (after) the MIE transition. The MIE was also found to increase monotonically with turbulent intensity via three-dimensional (3D) DNS considering one-step chemistry [11,12] and detailed chemistry [13].

However, Law and co-workers [4] found the counterintuitive turbulence-facilitated ignition (TFI) in a fuel-rich ($\phi=5.1$) hydrogen/air mixture whose effective/global Lewis number is $Le\approx 2.3$ and in a fuel-lean ($\phi=0.7$) butane/air mixture with $Le\approx 2.1$. They attributed the TFI to the facts that turbulence breaks the single, highly positively stretched, ignition kernel into many wrinkled flame elements with both positive and negative stretch, and that the intensified burning of the flame segments with negative stretch at $Le > 1$ helps to promote ignition [4]. TFI was also observed in other experimental studies [14–17], which showed that TFI only occurs at sufficiently large Le and moderate turbulence intensity. However, TFI has not yet been observed in simulations. The most related numerical study is the DNS of ignition kernel evolution in a turbulent H_2 /air mixture with $\phi=4$ and $Le\approx 2.15$ conducted by Uranakara et al. [18]. This study showed that turbulence locally wrinkles the flame front into more positively stretched structures and thereby renders ignition more difficult, which is in contradiction to the interpretation of TFI mentioned above. The reason for such contradictory findings from experiments and simulations is still not clear, which motivates the present study.

Compared to spark ignition in experiments, usually several simplifications with respect to the spark are made in numerical studies. For instance, in the simulations by Uranakara et al. [18], the ignition kernel was represented by a small high-temperature region. The electrodes and the heat loss to them were not considered, which could be one reason for not observing TFI in [18]. Recently, Shy and coworkers [14,15,17] assessed the effects of electrode gap distance on ignition kernel development and found that TFI occurs only for relatively small gap distance. They emphasized the important role of heat loss to electrodes, and suggested that weak turbulence may blow the ignition kernel away from the electrodes and thereby reduce the heat loss to the electrodes, leading to TFI.

In summary, the previous experiments concluded that TFI occurs only for mixtures with large Lewis number ($Le \gg 1$) and small gap distance between two electrodes ($d_{gap} < 2$ mm). Furthermore, the negative stretch and the reduction in heat loss to electrodes, both induced by weak turbulence, were identified as two important factors that lead to TFI. Nevertheless, the individual contributions of the two factors to TFI as well as the underlying TFI mechanisms are still not well understood.

In this context, the objective of this study is to assess the effects of heat loss to electrodes, curvature/Lewis number interaction and flow around electrodes on the ignition kernel development in laminar premixed hydrogen/air mixtures. Note that including electrodes in the simulations not only introduces heat loss but also affects the shape and local curvature or stretch rate of the ignition kernel. The flowing mixture is considered to mimic the local turbulent flow around the electrodes which blows the ignition kernel away from the electrodes. Though turbulence is not considered here, this work is a first step to numerically assess the mechanism responsible for TFI through simulating forced ignition in laminar flows which helps to isolate multiple factors involved in TFI. Since TFI occurs only for large Le , here we mainly consider a fuel-rich ($\phi=5.1$) H_2 /air mixture with $Le\approx 2.3$. Both 2D and 3D simulations considering detailed chemistry and transport are conducted to investigate the transient ignition kernel evolution.

2. Model and numerical methods

We consider the forced ignition induced by a pair of fixed electrodes in initially quiescent or flowing H_2 /air mixture at $T_0=298$ K and $P=1$ atm. Unless otherwise specified, the equivalence ratio is $\phi=5.1$ and thereby $Le\approx 2.3$. For the quiescent mixture, the configuration is axisymmetric along the center line of the electrodes (see Fig. 1a), and thereby 2D simulations are conducted. For the flowing mixture, the imposed flow is oriented perpendicular to the electrodes (see Fig. 1b) and

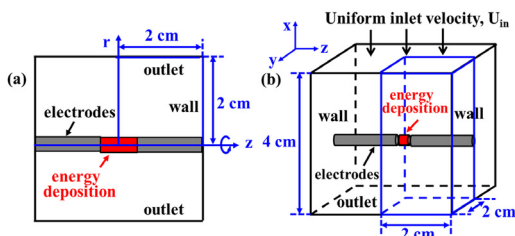


Fig. 1. Schematics of the (a) 2D and (b) 3D simulation setup. The blue rectangle and cuboid represent the computational domains in 2D and 3D simulations, respectively.

thereby 3D simulations are performed. Due to symmetry, the computational domain is a quarter of the whole region shown in Fig. 1, in which the boundary conditions as well as the dimensions are also depicted. For the flowing mixture, a uniform inlet velocity, U_{in} , is prescribed at the top boundary (see Fig. 1b), and the steady cold flow field is used as the initial velocity field for the subsequent reactive flow simulations.

For simplicity, the electrical energy discharge process (e.g. the plasma formation, shock wave) is not considered in the simulations. We assume that the ignition energy is released uniformly in the cylindrical space between the two electrodes (see the red region in Fig. 1) at a constant ignition energy density, q_{ig} , during the spark duration τ_{ig} . The ignition energy is:

$$E_{ig} = \pi R_e^2 d_{gap} \tau_{ig} q_{ig}, \quad (1)$$

where R_e is the radius of the electrodes and d_{gap} is the gap spacing between them. Here, we fix $\tau_{ig} = 0.2$ ms and $R_e = 0.32$ mm. Two gap distances, $d_{gap} = 0.64$ and 3.84 mm are chosen to assess the effects of the electrode gap on the ignition kernel evolution. At a specified ignition energy, the energy density, q_{ig} , can be evaluated according to Eq. (1) and it is included in the energy equation as a source term in all simulations.

At the electrode surface, there is no surface reaction and a non-slip boundary condition is enforced. Unless otherwise indicated, an isothermal boundary with fixed surface temperature, $T_s = 298$ K, is used for the electrodes and thereby there is heat loss to the electrodes. Note that due to high heat capacity of the electrodes and short ignition time, the temperature of electrodes is assumed to be constant. This is demonstrated in the Supplementary Document.

2D and 3D simulations of the transient ignition process are conducted using an OpenFOAM-based solver developed by Zirwes et al. [19,20]. The finite volume method is used to solve the compressible conservation equations for multi-component reactive flows. The detailed chemistry for hydrogen developed by Li et al. [21] is used. Cantera

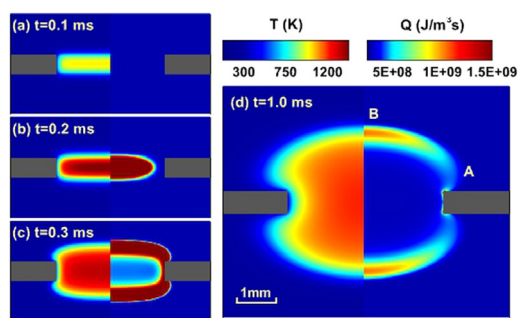


Fig. 2. Evolution of ignition kernel at (a) $t = 0.1$ ms, (b) $t = 0.2$ ms, (c) $t = 0.3$ ms and (d) $t = 1.0$ ms in a H_2 /air mixture with $\phi=5.1$, $d_{gap}=3.84$ mm and $E_{ig}=1.24$ mJ. Each subfigure shows the temperature (left) and heat release rate (right) contours.

[22] is incorporated to calculate the reaction rates as well as transport coefficients. The mixture-averaged model is used to evaluate the mass diffusivities for all species. This code has been successfully used in recent studies on premixed flames [23,24]. Details on numerical schemes and code validation can be found in [19,20].

In all simulations, a non-uniform mesh is adopted and the size of the finest cell is 16 μ m. During the ignition kernel development, the reaction front is always resolved by more than 30 grid points so that grid convergence is ensured.

3. Ignition in quiescent mixtures

According to experiments by Shy et al. [14,15,17], the unusual TFI phenomenon occurs only at sufficiently small d_{gap} and at sufficiently large Le . In this section, the effects of electrodes and Lewis number on ignition kernel development are assessed by considering ignition in quiescent H_2 /air mixtures.

The forced ignition process consists of four phases: ignition kernel formation, ignition kernel growth into a flame kernel, transition from a flame kernel to a self-sustained propagating flame, and flame stabilization. Here the initial ignition kernel is formed due to an ignition energy deposition (complex plasma chemistry is not considered). In Fig. 2, the ignition kernel growth and the flame kernel transition to a propagating flame are shown for a successful ignition case with $\phi=5.1$, $d_{gap}=3.84$ mm and $E_{ig}=1.24$ mJ. The final flame stabilization is not considered.

Due to the ignition energy deposition, the gaseous mixture between two electrodes is heated up. Fig. 2(a) shows that at $t = 0.1$ ms, the temperature of the ignition kernel is around 1000 K but the chemical heat release rate remains negligible since autoignition still does not occur. The large temper-

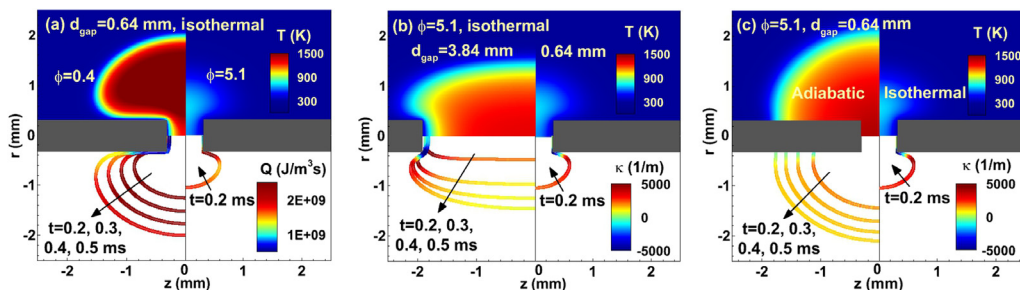


Fig. 3. Evolution of the ignition kernel in H_2 /air mixtures at the same ignition energy of $E_{ig} = 1.24$ mJ but (a) different equivalence ratios with $\phi = 0.4$ (left) and 5.1 (right), (b) different gap distances with $d_{gap} = 3.84$ mm (left) and 0.64 mm (right) and (c) different boundary conditions with adiabatic (left) and isothermal (right) boundary conditions on electrode surface. The reference case is: $\phi = 5.1$, $d_{gap} = 0.64$ mm considering isothermal electrodes, which is always provided on the right side. The upper frame shows the contour at $t = 0.5$ ms. The solid lines in the lower frame represent the evolution of reaction front (defined as the isosurface for $T = 700$ K) and their colors represent the magnitude of heat release rate, Q , or local curvature, κ . The arrow indicates the direction of flame kernel propagation and thereby successful and unsuccessful are achieved in the left and right frames, respectively.

ature gradient results in a large heat loss from the hot gas to the surrounding mixture as well as the cold electrodes. At $t = 0.2$ ms, autoignition occurs and there is intensive heat release, indicating that the ignition kernel is formed as shown in Fig. 2(b). At $t = 0.3$ ms, the mixture within the ignition kernel is rapidly consumed. Therefore, the ignition kernel in Fig. 2(b) evolves into an outwardly propagating flame kernel (Fig. 2c) with a thin reaction front and then it finally develops into a sustained propagating flame. The flame kernel in Fig. 2(d) is subjected to strong positive stretch rate. Since the positive stretch tends to weaken the reaction intensity for $Le > 1$ [25], the heat release rate around point A (with larger curvature and larger stretch) in Fig. 2(d) is much lower than that around point B (with smaller curvature and smaller stretch).

The above results indicate that in order to achieve successful ignition, sufficient energy should be deposited to ensure the following two processes: (1) autoignition occurring in the ignition kernel, (2) flame kernel transition into a self-sustained flame. In the first process, the electrodes can have a great impact since the heat loss to them could suppress autoignition. In the second process, the flame kernel needs to overcome the combined effects between stretch and Lewis number and reach a critical radius. The electrodes can affect the shape of the flame kernel and local stretch. Therefore, the second process is affected by both, the electrodes and the Lewis number.

To demonstrate the influence of Lewis number and electrodes on forced ignition, we compare the ignition kernel development in H_2 /air mixtures with the same ignition energy of $E_{ig} = 1.24$ mJ but different equivalence ratios (different Le) and different electrode characteristics (different d_{gap} and boundary condition at the surface). The results are shown in Fig. 3. The reference case is: $\phi = 5.1$,

$d_{gap} = 0.64$ mm considering isothermal electrodes, for which the results are provided on the right side.

To demonstrate the effects caused by the coupling between curvature/stretch and Lewis number, Fig. 3(a) compares the results for two equivalence ratios, $\phi = 0.4$ and 5.1 . At the same ignition energy, successful ignition is achieved for $\phi = 0.4$ with $Le \approx 0.43$, while ignition fails for $\phi = 5.1$ with $Le \approx 2.3$. This is because the positive stretch of the ignition kernel enhances and prohibits the flame ignition and propagation for $Le < 1$ and $Le > 1$, respectively [25,26]. The change of the local heat release rate with the equivalence ratio can also be explained by the stretch-chemistry interaction studied in [27,28].

Besides Le , the electrode characteristics such as material, shape, diameter and gap distance can also affect the ignition process. Shy et al. [14] showed that the occurrence of TFI is almost independent of the electrode shape (flat end or sharp end) and diameter (0.25 mm and 2 mm). Therefore, here we only assess effects of gap distance, d_{gap} , and electrode materials. Fig. 3(b) compares the results for $d_{gap} = 3.84$ mm (successful ignition) and $d_{gap} = 0.64$ mm (failed ignition). Increasing d_{gap} helps to generate a large ignition kernel at the very beginning, which reduces the heat loss to electrodes. Besides, after increasing d_{gap} , the initial kernel transforms from a ball-like shape with high curvature/stretch to a rod-like shape with small or negligible curvature/stretch (see Fig. 3b). Consequently, it is easier for the ignition kernel to evolve into a self-sustained propagating flame at larger d_{gap} .

The material of the electrodes determines the heat loss from the initial kernel to the electrodes. Fig. 3(c) compares the results for two limiting cases with adiabatic and isothermal boundary conditions imposed at the electrode surface. Successful and

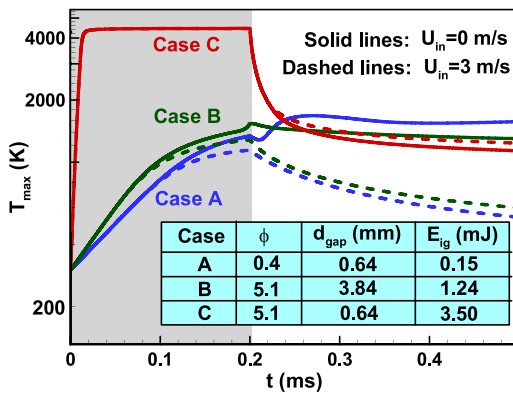


Fig. 4. Evolution of the maximum temperature during the ignition kernel development in quiescent (solid lines) and flowing (dashed lines) H_2 /air mixtures. The ignition energies for cases A-C are close to the respective minimum ignition energy.

unsuccessful ignition is achieved, respectively. For the isothermal electrodes, the temperature of the ignition kernel is greatly reduced by heat loss to the electrodes. Furthermore, the reaction front in the axial direction is wrinkled into a more positively curved structure by the huge heat loss to the isothermal electrodes, which further prohibits the ignition kernel development for $Le > 1$. Therefore, the heat loss to the electrodes plays an important role in the ignition of mixtures with large Le . In previous simulations (e.g., [18]) of ignition phenomena in mixtures with large Le , the electrodes and the heat loss to them were not considered, and thereby TFI cannot be observed.

In summary, the positive stretch/curvature and heat loss to the electrodes cause ignition failure for the reference case with large Le , small d_{gap} , and isothermal electrodes (i.e., Case C: $\phi=5.1$, $Le \approx 2.3$, $d_{gap}=0.64$ mm). Reducing Le (i.e., Case A: $\phi=0.4$, $Le \approx 0.43$, $d_{gap}=0.64$ mm) or increasing d_{gap} (i.e., Case B: $\phi=5.1$, $Le \approx 2.3$, $d_{gap}=3.84$ mm) helps to achieve successful ignition as shown in Fig. 3. The MIE for cases A and B is 0.15 mJ and 1.24 mJ, respectively. For the reference case C, ignition still fails when the ignition energy is increased to 3.50 mJ. The temporal evolution of the maximum temperature for these three cases are shown in Fig. 4.

As mentioned before, the MIE is required to ensure two processes: (1) autoignition occurring in the ignition kernel, (2) flame kernel transition into a self-sustained flame. For case A with $Le < 1$, the positive curvature of the flame kernel increases the local reactivity and thereby promotes the flame kernel transition into a self-sustained flame. For case B with $Le > 1$, the rod-like flame kernel exhibits a very low curvature/stretch in z-direction (see the left frame of Fig. 3b) and thus can easily propagate outwardly. Consequently, the MIE for cases A and B is

mainly determined by the first process, i.e., the maximum temperature only needs to be high enough to trigger autoignition. Therefore, Fig. 4 shows that successful ignition is achieved for cases A and B with relatively low ignition energy. However, the MIE for case C is mainly determined by the second process since the large Le and high positive curvature/stretch greatly inhibit the flame kernel development. Consequently, the MIE for case C is much larger than that for cases A and B. Fig. 4 shows that though the maximum temperature above 4000 K is high enough to ensure autoignition in the ignition kernel, ignition still fails since the flame kernel cannot transition into a self-sustained flame.

4. Ignition in mixtures with imposed flow

In this section, we consider the effects of flow around the electrodes and its coupling with the Lewis number effect and heat loss to electrodes. Cases A-C listed in Fig. 4 are chosen in the following discussion. Fig. 5 compares the ignition kernel evolution in

Note that Fig. 5 only shows the results on the plane at $y = 0$ mm. The 3D ignition kernel evolution is shown in Fig. 6 for case C with $U_{in}=3$ m/s. An animation of the ignition kernel development for cases A-C is shown in the Supplementary Material.

To understand the mechanisms behind the influence of the inlet flow on ignition, in the following we shall investigate how the imposed flow changes heat transfer and flame curvature, both of which are very important for ignition and help to explain TFI.

4.1. Effects of inlet flow on heat transfer

For forced ignition in a flowing mixture, the convective heat loss induced by imposed flow and the conductive heat transfer from the hot ignition kernel to the cold electrodes are two main sources of energy loss. To quantify these two effects, we conduct an energy budget analysis by evaluating the following convective and conductive terms in the energy equation:

$$E_{Conv} = -\rho C_p u_i \frac{\partial T}{\partial x_i}, E_{Cond} = -\frac{\partial}{\partial x_i} \left(\lambda \frac{\partial T}{\partial x_i} \right) \quad (2)$$

Fig. 7 shows the contours of these two terms at the end of the energy deposition, i.e., $t = 0.2$ ms for cases A-C. The corresponding temperature contours are shown in Fig. 5(a1), (b1) and (c1), respectively. For cases A and B, autoignition has not occurred yet at $t = 0.2$ ms. Fig. 7(a) and (b) clearly show that before autoignition, there is a strong convective heat transfer from the hot ignition kernel to the unburned mixture downstream. Compared to the successful ignition in the quiescent mixture, ignition fails in the flowing mixture (see Fig. 5a). This

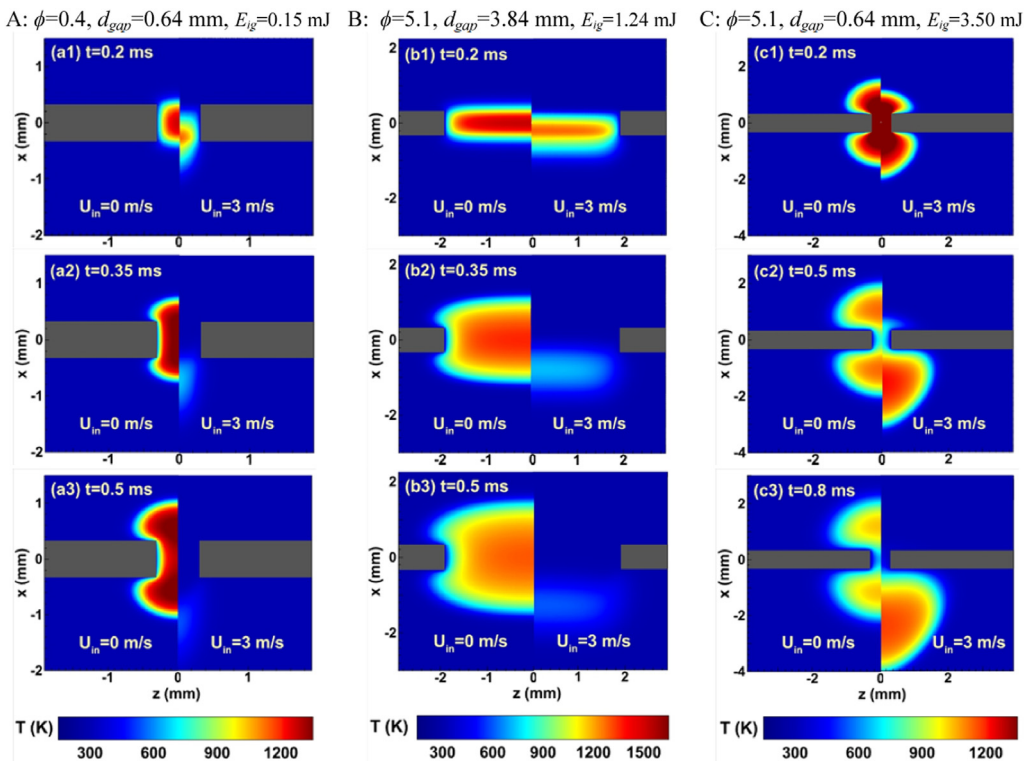


Fig. 5. Evolution of the temperature contours during ignition in quiescent (left, $U_{in}=0$ m/s) and flowing (right, $U_{in}=3$ m/s) H_2 /air mixtures for Case A (left column), Case B (middle column) and Case C (right column). quiescent ($U_{in}=0$ m/s) and flowing ($U_{in}=3$ m/s) H_2 /air mixture for cases A-C. The evolution of the maximum temperature is compared in Fig. 4. Figs. 4 and 5 show that the inlet flow renders ignition more difficult for cases A and B, while it promotes ignition for case C. This observation is similar to previous experimental findings on ignition in turbulent flows, where TFI only occurs at very large Le and sufficiently small d_{gap} [14–17].

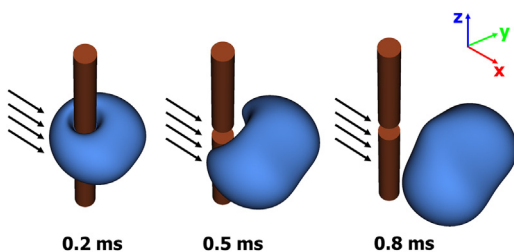


Fig. 6. Evolution of the ignition kernel for case C at $t = 0.2, 0.5$ and 0.8 ms.

is because the temperature of the ignition kernel is reduced by the extra convective heat loss and, consequently, autoignition cannot occur after the energy deposition. However, for case C, the ignition kernel is initiated with a considerably large ignition energy. Fig. 4 shows that the maximum temperature reaches around 4000 K at $t = 0.05$ ms for case C, and thereby autoignition readily occurs before $t = 0.2$ ms even when there is convective heat loss

due to the enforced flow. Therefore, the autoignition process of case C is not affected by the enforced flow. After autoignition, the ignition kernel evolves into a flame kernel at $t = 0.2$ ms. The thermal expansion due to the hot flame kernel partly encounters the enforced inlet flow and changes the surrounding flow field. Therefore, in Fig. 7(c), low convective heat loss is observed within the flame kernel. However, due to the high temperature of the ignition kernel in case C, the conductive heat loss at the electrode surface is much stronger than that in the other two cases. When the inlet flow blows the flame kernel away from the electrodes, the area of electrode contact surface decreases and thereby the conductive heat loss to the electrodes is greatly reduced. In the subsequent propagation stage, the flame kernel can survive more easily when it is blown away from the cold electrodes. Otherwise, in the quiescent environment, the flame kernel is quenched due to the heat losses to the electrodes (see Fig. 3c).

Therefore, Fig. 7 clearly shows that the imposed flow has both positive and negative effects on the

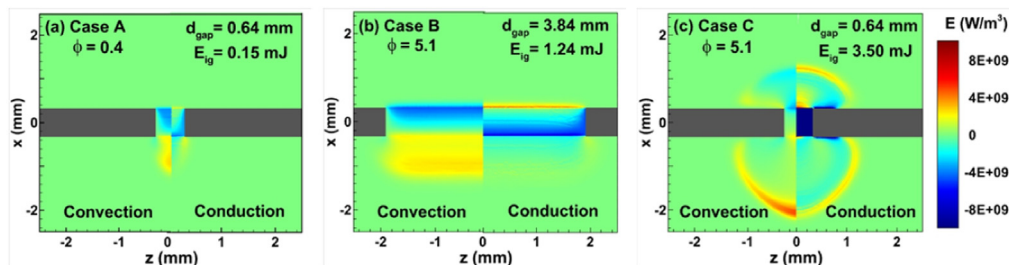


Fig. 7. Contours of convective and conductive terms in energy equation at $t = 0.2$ ms and in flowing H_2 /air mixture with $U_{in}=3$ m/s.

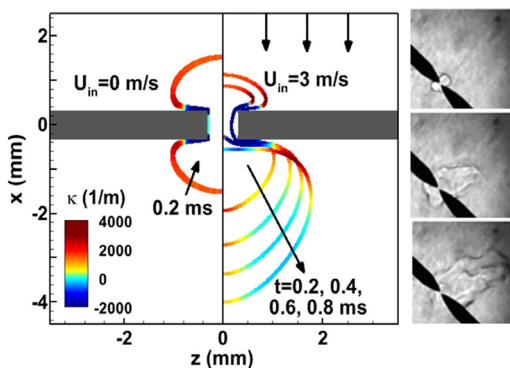


Fig. 8. Evolution of the reaction front (defined with temperature isosurface of 700 K) in quiescent (left, $U_{in}=0$ m/s) and flowing (right, $U_{in}=3$ m/s) H_2 /air mixtures for case C. The color represents the magnitude of curvature. The photos in the right column are from Fig. 6 in Ref. [15], which were from experiments on ignition in turbulent flow by Shy et al.

heat transfer from the ignition kernel. The negative effect originates from the convective dissipation of the deposited energy during the autoignition stage (see Fig. 7a-b), while the positive effect is based on the fact that the inlet flow may blow the ignition kernel away from the spark gap and thereby reduces the conductive heat loss to the electrodes during the ignition kernel propagation stage (see Fig. 7c).

4.2. Effects of inlet flow on flame curvature

Besides the change in heat transfer induced by the inlet flow, the geometry of the initial kernel is also modified by the inlet flow. Shy et al. [17] found that the initial kernel geometry determines the curvature of the subsequent flame kernel. For large Le , the curvature (or stretch) has great impact on flame propagation speed. Therefore, the change in the flame kernel curvature induced by the inlet flow can greatly affect the ignition process.

Fig. 8 shows that enforcing an inlet flow breaks the symmetry of the ignition kernel. Compared to the flame kernel in the quiescent mixture, the flame

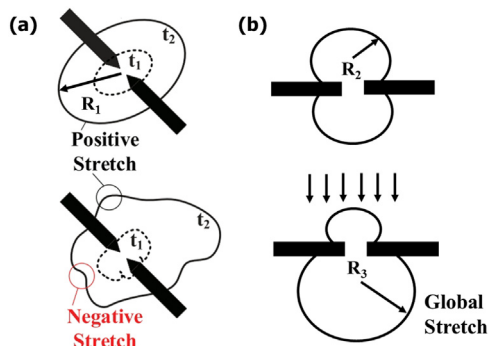


Fig. 9. Schematics of the ignition kernel in (a) intensive turbulence and (b) uniform flow. Subfigure (a) is from Fig. 6 in Ref. [15].

kernel downstream in the flowing environment has a much smaller curvature and thereby can successfully propagate outwardly even for $Le \gg 1$. It is the reduction in curvature/stretch that allows the imposed flow to promote ignition in a mixture with large Le . In practical combustion facilities such as spark ignition (SI) gasoline engines, the most common scenario is to burn fuel-lean heavy hydrocarbon/air mixtures which also have large Le . Therefore, the present findings indicate that the misfire problem relevant to lean-burn large hydrocarbons in SI gasoline engines can possibly be improved by local flow when the electrode gap is small. In future works, the forced ignition in a flowing fuel-lean heavy hydrocarbon/air mixture needs to be considered

The schematics of the ignition kernel in intensive turbulence and uniform flow are further shown in Fig. 9. In previous experimental studies [4,14-17], the local negative stretch rate (see Fig. 9a), induced by the weak turbulence was identified to be responsible for the occurrence of TFI. However, previous numerical study [18] showed that turbulence locally wrinkles the flame front into more positively stretched structures (see Fig. 9a) and thereby renders ignition more difficult. So far, previous studies all focused on the change in local stretch

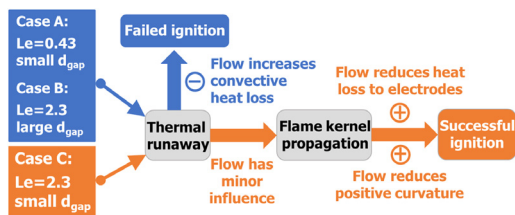


Fig. 10. Positive (circle+) and negative (circle-) effects induced by the flow around the electrodes. The blue and red arrows represent the ignition pathway for failed and successful ignition, respectively.

rate of the wrinkled ignition kernel and there are contradictory findings from experiments and numerical simulations. In this study, the importance of the coupled effects of heat loss to electrodes and local flow around the electrodes in the occurrence of TFI is emphasized. It is found that the heat loss to electrodes has both a thermal and a kinetic effect on the ignition kernel evolution. Thermal suppression is achieved by decreasing the temperature of the ignition kernel via heat conduction from ignition kernel to cold electrodes. Kinetic suppression is accomplished by wrinkling the reaction front of ignition kernel into a more positively curved structure and thereby increases the global curvature of the ignition kernel (i.e. $1/R_2 > 1/R_1$ in Fig. 9). The above results in flowing mixtures indicate that in TFI experiments, the local turbulent flow may blow the ignition kernel away from the electrodes (see the photos in the right column of Fig. 8 as well as Fig. 6 in [15]) and thereby promotes ignition by reducing the heat loss to electrodes and decreasing the global curvature of the flame kernel (i.e. $1/R_3 < 1/R_2$ in Fig. 9b). This explains the basic physical phenomena causing TFI for mixtures with large Le . In recent laser-induced spark ignition experiments by Shy et al. [29], TFI was not observed when electrodes were not present. This could be an evidence that supports our present findings.

In a brief summary, the imposed flow has significant impact on ignition depending on the Lewis number and gas distance between the electrodes. The influence of imposed flow is summarized in Fig. 10.

5. Conclusions

In this study, 2D and 3D simulations are conducted to study the forced ignition in hydrogen/air mixtures with large Lewis number. The combined effects of heat losses, curvature-induced Lewis number effects, and flow around the electrodes on the ignition kernel development are investigated.

First, the effects of electrodes and Lewis number effects on ignition are examined by considering ignition in quiescent fuel-rich ($\phi=5.1$, $Le\approx 2.3$)

and fuel-lean ($\phi=0.4$, $Le\approx 0.43$) H_2 /air mixtures using the same ignition energy. It is found that, in order to achieve successful ignition, two processes need to be proceeded successfully: (1) autoignition occurring in the ignition kernel, and (2) the flame kernel transition into a self-sustained flame. Autoignition is mainly dominated by heat transfer and is greatly affected by heat losses to the electrodes. The flame kernel transition is determined by the coupling between flame curvature/stretch and Lewis number effects. It is shown that the large positive curvature/stretch of the ignition kernel prohibits or enhances ignition for fuel-rich and fuel-lean H_2 /air mixtures, respectively. Increasing the gap distance between electrodes, d_{gap} , helps to reduce the heat losses to the electrodes as well as the curvature/stretch of the ignition kernel, and thereby it can promote ignition for mixtures with large Le . Besides, at the same ignition energy, successful and unsuccessful ignition is shown to be achieved for adiabatic and isothermal electrodes, demonstrating that the heat loss to the electrodes plays an important role during the ignition. Consequently, in simulations without considering the electrodes (e.g., [18]) and the heat loss to them could be one reason for not observing TFI in mixtures with large Le .

Further, the effects of flow around the electrodes are assessed via 3D simulations of ignition in a flowing H_2 /air mixture. It is found that the inlet flow inhibits ignition for case A with small Le and small d_{gap} and case B with large Le and large d_{gap} , while it promotes ignition for case C with large Le and small d_{gap} . This observation agrees with experimental findings on the ignition in turbulent flows that TFI only occurs at large Le and small d_{gap} . An energy budget analysis shows that the inlet flow has both positive and negative effects on the heat transfer from the ignition kernel. As summarized in Fig. 10, for cases A and B, the ignition inhibition by the inlet flow is attributed to the convective heat loss of the deposited energy, which suppresses the occurrence of autoignition. However, for case C, with a large Le and a small d_{gap} , a large ignition energy is required to ensure successful ignition. For such cases, autoignition is easily obtained during the energy deposition period and thereby is not affected by the convective heat loss. The ignition is controlled by the flame kernel transition stage after autoignition. The inlet flow normal to the electrodes tends to blow the flame kernel away from the cold electrodes, reducing the heat loss to the electrodes significantly and modifying the geometry of the flame kernel into a shape with a smaller positive curvature. Both effects promote the subsequent flame kernel propagation.

In the experiments of Shy et al. [14,15,17], the local turbulent flow was observed to blow the ignition kernel away from the electrodes, too. According to this study, such movement of the igni-

tion kernel can greatly reduce both the heat loss to the electrodes and flame curvature/stretch, and thereby promotes ignition in mixture with large Le . In summary, this work partly explains the underlying TFI mechanisms by investigating the impact of heat losses to and the flow around the electrodes on ignition. Certainly, complete understanding and interpretation of the TFI require simulations considering the turbulent rather than laminar flows. This needs to be explored in future studies. Besides, here the ignition kernel is induced by uniform energy deposition in the cylindrical space between the two electrodes. The formation of ignition kernel [30–32] also affects the ignition process and thereby its coupling with laminar or turbulent flow needs to be studied in the future.

Supplementary material

A supplementary material containing animations of ignition kernel development is provided.

Declaration of Competing Interest

The authors declare that they have no known competing financial interests or personal relationships that could have appeared to influence the work reported in this paper.

Acknowledgements

This research was jointly funded by NSFC (No. 51861135309) and DFG (No. 411275182). Calculations for this research were conducted on the Lichtenberg II High Performance Computer of the Technical University of Darmstadt. We thank Drs. Thorsten Zirwes, Feichi Zhang, and Henning Bockhorn at Karlsruhe Institute of Technology, for providing us their code. Z.C. thanks Prof. S.S. Shy for helpful discussion and for permitting us to use some figures from his publication.

Supplementary materials

Supplementary material associated with this article can be found, in the online version, at doi:10.1016/j.proci.2022.07.217.

References

- [1] E. Mastorakos, Forced ignition of turbulent spray flames, *Proc. Combust. Inst.* 36 (2017) 2367–2383.
- [2] R.D. Reitz, Directions in internal combustion engine research, *Combust. Flame* 160 (2013) 1–8.
- [3] N. Saito, Y. Minamoto, B. Yenerdag, M. Shimura, M. Tanahashi, Effects of turbulence on ignition of methane–air and n-heptane–air fully premixed mixtures, *Combust. Sci. Technol.* 190 (2018) 452–470.
- [4] F. Wu, A. Saha, S. Chaudhuri, C.K. Law, Facilitated ignition in turbulence through differential diffusion, *Phys. Rev. Lett.* 113 (2014) 024503.
- [5] C.C. Huang, S.S. Shy, C.C. Liu, Y.Y. Yan, A transition on minimum ignition energy for lean turbulent methane combustion in flamelet and distributed regimes, *Proc. Combust. Inst.* 31 (2007) 1401–1409.
- [6] S.S. Shy, C.C. Liu, W.T. Shih, Ignition transition in turbulent premixed combustion, *Combust. Flame* 157 (2010) 341–350.
- [7] C.C. Liu, S.S. Shy, H.C. Chen, M.W. Peng, On interaction of centrally-ignited, outwardly-propagating premixed flames with fully-developed isotropic turbulence at elevated pressure, *Proc. Combust. Inst.* 33 (2011) 1293–1299.
- [8] M.W. Peng, S.S. Shy, Y.W. Shiu, C.C. Liu, High pressure ignition kernel development and minimum ignition energy measurements in different regimes of premixed turbulent combustion, *Combust. Flame* 160 (2013) 1755–1766.
- [9] S.S. Shy, Y.W. Shiu, L.J. Jiang, C.C. Liu, S. Minaev, Measurement and scaling of minimum ignition energy transition for spark ignition in intense isotropic turbulence from 1 to 5 atm, *Proc. Combust. Inst.* 36 (2017) 1785–1791.
- [10] C. Cardin, B. Renou, G. Cabot, A.M. Boukhalfa, Experimental analysis of laser-induced spark ignition of lean turbulent premixed flames: new insight into ignition transition, *Combust. Flame* 160 (2013) 1414–1427.
- [11] T. Poinso, Using direct numerical simulations to understand premixed turbulent combustion, *Symp. (Int.) Combust.* 26 (1996) 219–232.
- [12] M. Klein, N. Chakraborty, R. Cant, Effects of turbulence on self-sustained combustion in premixed flame kernels: a direct numerical simulation (DNS) study, *Flow Turbul. Combust.* 81 (2008) 583–607.
- [13] C. Chi, A. Abdelsamie, D. Thévenin, Direct numerical simulations of hotspot-induced ignition in homogeneous hydrogen–air pre-mixtures and ignition spot tracking, *Flow Turbul. Combust.* 101 (2018) 103–121.
- [14] S.S. Shy, M.T. Nguyen, S.Y. Huang, C.C. Liu, Is turbulent facilitated ignition through differential diffusion independent of spark gap? *Combust. Flame* 185 (2017) 1–3.
- [15] S.S. Shy, M.T. Nguyen, S.Y. Huang, Effects of electrode spark gap, differential diffusion, and turbulent dissipation on two distinct phenomena: turbulent facilitated ignition versus minimum ignition energy transition, *Combust. Flame* 205 (2019) 371–377.
- [16] A. Saha, S. Yang, C.K. Law, On the competing roles of turbulence and differential diffusion in facilitated ignition, *Proc. Combust. Inst.* 37 (2019) 2383–2390.
- [17] S.S. Shy, Y.C. Liao, Y.R. Chen, S.Y. Huang, Two ignition transition modes at small and large distances between electrodes of a lean primary reference automobile fuel/air mixture at 373K with Lewis number $>> 1$, *Combust. Flame* 225 (2021) 340–348.
- [18] H.A. Uranakara, S. Chaudhuri, K.N. Lakshminisha, On the extinction of igniting kernels in near-isotropic turbulence, *Proc. Combust. Inst.* 36 (2017) 1793–1800.
- [19] T. Zirwes, F. Zhang, J.A. Denev, P. Habisreuther, H. Bockhorn, in: Automated Code Generation for Maximizing Performance of Detailed Chemistry Calculations in openfoam, *High Performance Com-*

- puting in Science and Engineering, 17, Springer International Publishing, Cham, 2018, pp. 189–204.
- [20] T. Zirwes, F. Zhang, P. Habisreuther, M. Hansinger, H. Bockhorn, M. Pfitzner, D. Trimis, Quasi-DNS dataset of a piloted flame with inhomogeneous inlet conditions, *Flow Turbul. Combust.* 104 (2020) 997–1027.
- [21] J. Li, Z. Zhao, A. Kazakov, F.L. Dryer, An updated comprehensive kinetic model of hydrogen combustion, *Int. J. Chem. Kinet.* 36 (2004) 566–575.
- [22] D.G. Goodwin, *Cantera C++ User's Guide*, California Institute of Technology, 2002.
- [23] X. Chen, Y. Wang, T. Zirwes, F. Zhang, Z. Chen, Heat release rate markers for highly stretched premixed CH₄/air and CH₄/H₂/air flames, *Energy Fuels* 35 (2021) 13349–13359.
- [24] Y. Wang, H. Zhang, T. Zirwes, F. Zhang, H. Bockhorn, Z. Chen, Ignition of dimethyl ether/air mixtures by hot particles: impact of low temperature chemical reactions, *Proc. Combust. Inst.* 38 (2021) 2459–2466.
- [25] C.K. Law, *Combustion Physics*, Cambridge University Press, 2006.
- [26] Z. Chen, M.P. Burke, Y. Ju, On the critical flame radius and minimum ignition energy for spherical flame initiation, *Proc. Combust. Inst.* 33 (2011) 1219–1226.
- [27] K.T. Aung, M.I. Hassan, G.M. Faeth, Flame stretch interactions of laminar premixed hydrogen/air flames at normal temperature and pressure, *Combust. Flame* 109 (1997) 1–24.
- [28] X. Chen, H. Böttler, A. Scholtissek, C. Hasse, Z. Chen, Effects of stretch-chemistry interaction on chemical pathways for strained and curved hydrogen/air premixed flames, *Combust. Flame* 232 (2021) 111532.
- [29] Y.R. Chen, S.S. Shy, Can the phenomenon of turbulence facilitated ignition through differential diffusion occur in laser-induced spark ignition? *Combust. Flame* 242 (2022) 112165.
- [30] D. Yu, X. Chen, Z. Chen, Analysis on ignition kernel formation in a quiescent mixture: different characteristic time scales and critical heating powers, *Combust. Flame* 245 (2022) 112326.
- [31] X. Mao, H. Zhong, Z. Wang, T. Ombrello, Y. Ju, Effects of inter-pulse coupling on nanosecond pulsed high frequency discharge ignition in a flowing mixture, *Proc. Combust. Inst.* (2022) In press, doi:10.1016/j.proci.2022.06.018.
- [32] D. Yu, Z. Chen, Theoretical analysis on the forced ignition of a quiescent mixture by repetitive heating pulse, *Proc. Combust. Inst.* 39 (2022) in press, doi:10.1016/j.proci.2022.06.014.